Research Article | Vol. 25, No. 24 | 27 Nov 2017 | OPTICS EXPRESS 30336
Optics EXPRESS

200 Gb/s transmission using a dual-polarization O-Band silicon photonic intensity modulator for Stokes vector direct detection applications

ESLAM EL-FIKY,[1,2,*] MOHAMED OSMAN,[1,2] MOHAMMED SOWAILEM,[1] ALIREZA SAMANI,[1] DAVID PATEL,[1] RUI LI,[1] MD. G. SABER,[1] YUN WANG,[1] NICOLAS ABADIA,[1] YANNICK D'MELLO,[1] AND DAVID V. PLANT[1]

[1]*Department of Electrical and Computer Engineering, McGill University, Montreal, Quebec, H3A 0E9, Canada*
[2]*Electrical Engineering Department, Alexandria University, Alexandria, 21544, Egypt*
**eslam.elfiky@mail.mcgill.ca*

Abstract: We present a dual-polarization O-band silicon photonic (SiP) transmitter for intra-datacenter optical interconnects. The transmitter is built using two identical O-band traveling wave Mach-Zehnder modulators with an average $V_\pi L$ and a bandwidth at 1.5 V bias voltage of 2.88 V.cm and 24.5 GHz, respectively. We experimentally demonstrate the transmitter in a Stokes vector direct-detection (SV-DD) system for dual-polarization intensity modulated signals with 2-level and 4-level pulse amplitude modulation (DP-PAM2 and DP-PAM4) formats. The direct-detection Stokes vector receiver (DD-SVR) followed by offline digital signal processing (DSP) is implemented for SOP de-rotation. We characterize the performance of the SV-DD system versus number of taps, received signal power, state of polarization (SOP), reach, and bit rate. Results reveal that 112 Gb/s DP-PAM2 can be transmitted over 10 km of single mode fiber (SMF) at a bit error rate (BER) below 10^{-5} at −1 dBm received signal power irrespective of the SOP. Moreover, a 168 Gb/s (42 Gbaud) DP-PAM4 signal can be transmitted over 2 km and 10 km at a BER below the 7% hard-decision forward error correction (HD-FEC) threshold (i.e., 3.8×10^{-3}) at 0 dBm and 2 dBm, respectively. Furthermore, 224 Gb/s and 200 Gb/s DP-PAM4 are successfully received at a BER below the HD-FEC in the back-to-back and 2 km cases, respectively. Finally, we compare the performance of the 6×2 multiple-input multiple-output (MIMO) equalization to a simpler 4×2 MIMO equalization and explain the superior performance of the 6×2 in the presence of SVR imperfections.

OCIS codes: (130.3120) Integrated optics devices; (230.4110) Modulators; (200.4650) Optical interconnects.

References and links

1. "Cisco Global Cloud Index: Forecast and Methodology, 2015-2020," White Paper-c11-738085, 2016, http://www.cisco.com/c/dam/en/us/solutions/collateral/service-provider/global-cloud-index-gci/white-paper-c11-738085.pdf .
2. "IEEE Standard for Ethernet," IEEE Std 802.3-2015 .
3. "IEEE P802.3bs 200 Gb/s and 400 Gb/s Ethernet Task Force," http://www.ieee802.org/3/bs/index.html.
4. "IEEE P802.3bs Baseline Summary," http://www.ieee802.org/3/bs/baseline_3bs_0715.pdf .
5. "Ethernet alliance roadmap," http://www.ethernetalliance.org/roadmap .
6. D. Che, A. Li, X. Chen, Q. Hu, Y. Wang, and W. Shieh, "160-Gb/s stokes vector direct detection for short reach optical communication," in *Optical Fiber Communication Conference: Postdeadline Papers*, (Optical Society of America, 2014), paper Th5C.7.
7. D. Che, A. Li, X. Chen, Q. Hu, Y. Wang, and W. Shieh, "Stokes vector direct detection for short-reach optical communication," Opt. Lett. **39**(11), 3110–3113 (2014).
8. M. Morsy-Osman, M. Chagnon, M. Poulin, S. Lessard, and D. Plant, "1$\lambda\times$ 224 Gb/s 10 km transmission of polarization division multiplexed PAM-4 signals using 1.3 μm SiP intensity modulator and a direct-detection

#309573 https://doi.org/10.1364/OE.25.030336
Journal © 2017 Received 23 Oct 2017; accepted 30 Oct 2017; published 17 Nov 2017

Optics EXPRESS

MIMO-based receiver," in *Proceedings of European Conference on Optical Communication (ECOC)*, (IEEE, 2014), pp. 1–3.
9. P. Dumais, Y. Wei, M. Li, F. Zhao, X. Tu, J. Jiang, D. Celo, D. Goodwill, H. Fu, D. Geng, and eric Bernier, "2×2 multimode interference coupler with low loss using 248 nm photolithography," in *Optical Fiber Communication Conference*, (Optical Society of America, 2016), paper W2A.19.
10. E. Elfiky, A. Samani, D. Patel, and D. V. Plant, "A high extinction ratio, broadband, and compact polarization beam splitter enabled by cascaded MMIs on silicon-on-insulator," in *Optical Fiber Communication Conference*, (Optical Society of America, 2016), paper W2A.8.
11. D. Patel, S. Ghosh, M. Chagnon, A. Samani, V. Veerasubramanian, M. Osman, and D. V. Plant, "Design, analysis, and transmission system performance of a 41 GHz silicon photonic modulator," Opt. Express **23**(11), 14263–14287 (2015).
12. A. Samani, M. Chagnon, D. Patel, V. Veerasubramanian, S. Ghosh, M. Osman, Q. Zhong, and D. V. Plant, "A low-voltage 35-GHz silicon photonic modulator-enabled 112-Gb/s transmission system," IEEE Photon. J. **7**(3), 1–13 (2015).
13. J. S. Orcutt, D. M. Gill, J. Proesel, J. Ellis-Monaghan, F. Horst, T. Barwicz, C. Xiong, F. G. Anderson, A. Agrawal, Y. Martin, C. W. Baks, M. Khater, J. C. Rosenberg, W. D. Sacher, J. Hofrichter, E. Kiewra, A. D. Stricker, F. Libsch, B. Offrein, M. Meghelli, N. B. Feilchenfeld, W. Haensch, and W. M. J. Green, "Monolithic silicon photonics at 25 Gb/s," in *Optical Fiber Communication Conference*, (Optical Society of America, 2016), Th3H.1.
14. C. R. Doerr, L. Chen, D. Vermeulen, T. Nielsen, S. Azemati, S. Stulz, G. McBrien, X.-M. Xu, B. Mikkelsen, M. Givehchi, C. Rasmussen, and S. Y. Park, "Single-chip silicon photonics 100-Gb/s coherent transceiver," in *Optical Fiber Communication Conference: Postdeadline Papers*, (Optical Society of America, 2014), paper Th5C.1.
15. P. Dong, Chongjin Xie, and Lawrence L. Buhl, "Monolithic polarization diversity coherent receiver based on 120-degree optical hybrids on silicon," Opt. Express **22**(2), 2119–2125 (2014).
16. P. Dong, X. Chen, K. Kim, S. Chandrasekhar, Y.-K. Chen, and J. H. Sinsky, "128-Gb/s 100-km transmission with direct detection using silicon photonic stokes vector receiver and I/Q modulator," Opt. Express **24**(13), 14208–14214 (2016).
17. E. Elfiky, M. Sowailem, A. Samani, M. Osman, D. Patel, M. Chagnon, and D. V. Plant, "Dual polarization O-band silicon photonic intensity modulator for stokes vector direct detection systems," in *Optical Fiber Communication Conference*, (Optical Society of America, 2017), paper Tu2H.5.
18. A. Samani, V. Veerasubramanian, E. El-Fiky, D. Patel, and D. V. Plant, "A silicon photonic PAM-4 modulator based on dual-parallel Mach–Zehnder interferometers," IEEE Photon. J. **8**(1), 1–10 (2016).
19. Y. Zhang, S. Yang, A. E.-J. Lim, G.-Q. Lo, C. Galland, T. Baehr-Jones, and M. Hochberg, "A compact and low loss Y-junction for submicron silicon waveguide," Opt. Express **21**(1), 1310–1316 (2013).
20. J. H. Schmid, P. Cheben, M. Rahim, S. Wang, D.-X. Xu, M. Vachon, S. Janz, J. Lapointe, Y. Painchaud, M.-J. Picard, M. Poulin, and M. Guy, "Subwavelength gratings for broadband and polarization independent fiber-chip coupling with -0.4 db efficiency," in *Optical Fiber Communication Conference*, (Optical Society of America, 2016), paper M2I.4.
21. P. Cheben, J. H. Schmid, S. Wang, D.-X. Xu, M. Vachon, S. Janz, J. Lapointe, Y. Painchaud, and M.-J. Picard, "Broadband polarization independent nanophotonic coupler for silicon waveguides with ultra-high efficiency," Opt. Express **23**(17), 22553–22563 (2015).
22. M.-J. Picard, Y. Painchaud, C. Latrasse, C. Larouche, F. Pelletier, and M. Poulin, "Novel spot-size converter for optical fiber to sub-μm silicon waveguide coupling with low loss, low wavelength dependence and high tolerance to alignment," in "*Proceedings of European Conference on Optical Communication (ECOC)*," (IEEE, 2015), pp. 1–3.
23. G. Li, J. Yao, H. Thacker, A. Mekis, X. Zheng, I. Shubin, Y. Luo, J. hyoung Lee, K. Raj, J. E. Cunningham, and A. V. Krishnamoorthy, "Ultralow-loss, high-density SOI optical waveguide routing for macrochip interconnects," Opt. Express **20**(11), 12035–12039 (2012).
24. M. A. Guillén-Torres, M. Caverley, E. Cretu, N. A. Jaeger, and L. Chrostowski, Large-area, high-Q SOI ring resonators, in *Proceedings of IEEE Photonics Conference (IPC)*, (IEEE, 2014), pp. 336–337.
25. E. El-Fiky, M. Chagnon, M. Sowailem, A. Samani, M. Morsy-Osman, and D. V. Plant, "168 Gb/s single carrier PAM4 transmission for intra data center optical interconnects," IEEE Photon. Technol. Lett. **29**(3), 314-317, (2017).
26. M. Morsy-Osman, M. Chagnon, M. Poulin, S. Lessard, and D. V. Plant, "224-Gb/s 10-km transmission of PDM PAM-4 at 1.3 μm using a single intensity-modulated laser and a direct-detection MIMO DSP-based receiver," J. Lightw. Technol. **33**(7), 1417–1424 (2015).
27. S. Haykin, *Adaptive Filter Theory* (Pearson, 2008).
28. M. Chagnon, M. Osman, M. Poulin, C. Latrasse, J.-F. Gagné, Y. Painchaud, C. Paquet, S. Lessard, and D. Plant, "Experimental study of 112 Gb/s short reach transmission employing PAM formats and SiP intensity modulator at 1.3 μm," Opt. Express **22**(17), 21018–21036 (2014).

1. Introduction

The continuous increase in datacenter traffic has directed significant research effort towards developing high speed transceivers for intra-datacenter interconnects for reaches of 10 km and

Optics EXPRESS

less [1]. The 100G Ethernet standard for the 10 km single mode fiber (SMF) links and less which are currently being deployed stipulates 4 channels × 25 Gb/s non-return to zero (NRZ) signaling [2]. In addition, the IEEE 200 Gb/s and 400 Gb/s Ethernet Task Force has been working towards finalizing a 400 Gb/s Ethernet standard for the end of 2017 [3]. The selected solutions for single mode fiber links are 50 Gbaud 4-level pulse amplitude modulation (PAM4) × 4 parallel single mode (PSM) fibers for the 500 m reach, and 25 Gbaud PAM4 × 8 wavelength-division multiplexing (WDM) channels for the 2 and 10 km reaches [4]. According to the Ethernet alliance roadmap, future Ethernet speeds are envisioned to be 800 Gb/s and 1.6 Tb/s [5]. Assuming a bit rate of 100 Gb/s per channel, e.g., 50 Gbaud PAM4, 8 × 100 Gb/s and 16 × 100 Gb/s configurations are required using either PSM fibers or WDM to enable 800 Gb/s and 1.6 Tb/s, respectively. For the PSM configuration, 8 and 16 PSM fibers are needed per direction for the 800 Gb/s and 1.6 Tb/s, respectively. Hence, significant challenges will be faced for packaging in small form factors. On the other hand, 8 and 16 lasers in addition to a multiplexer at the transmitter side will be required for the 800 Gb/s and 1.6 Tb/s in the WDM case. This configuration will pose significant challenges on the thermal stability and packaging of optical transceivers. Hence, a scalable solution with rates beyond 100 Gb/s per channel is desirable for next generation optical interconnects.

Recently, a stokes vector receiver (SVR) has been proposed for self-coherent reception of single polarization complex modulated signals multiplexed with a tone on the other polarization [6, 7]. In [8], dual-polarization intensity modulation / direct-detection has been proposed and experimentally demonstrated using a SVR and novel digital signal processing (DSP). Using the polarization dimension and a direct-detection receiver offers a better scalable solution compared to single polarization PSM or WDM due to the reduction in the number of lasers required to achieve the same aggregate bit rate if the polarization dimension is exploited.

Along with the aforementioned challenges for future datacenter interconnects, silicon photonics (SiP) is emerging as a competitive platform for intra- and inter-datacenter optical transceivers. The SiP platform has the potential to build compact, high yield, high performance, and low cost complementary metal oxide semiconductor (CMOS) compatible transceivers. In the last few years, a plethora of SiP designs has been demonstrated ranging from device level demonstrations, e.g., multi-mode interference couplers [9], polarization beam splitters [10], traveling wave Mach-Zehnder modulators (TWMZMs) [11, 12], to system level demonstrations, e.g., 4 × 25 Gb/s WDM transceiver [13], and coherent transceivers [14, 15]. A C-band SiP SVR and an IQ modulator have been recently demonstrated targeting single polarization complex modulation with self-coherent detection for metro applications [16]. A 128 Gb/s quadrature amplitude modulated (16-QAM) signal over 100-km of SMF in the C-band, suitable for metro applications, below a bit error rate (BER) of 3.8×10^{-3} has been demonstrated [16].

In this paper, we present an O-band dual-polarization SiP transmitter based on TWMZMs in a stokes vector direct-detection (SV-DD) system targeting intra-datacenter applications. Preliminary experimental results of the SiP transmitter for only dual-polarization 2-level pulse amplitude modulated signaling (DP-PAM2) have been presented in [17]. In this paper, we report the DC characterization, small signal modulation, and large signal modulation of the SiP transmitter for both DP-PAM2 and DP 4-level pulse amplitude modulation (DP-PAM4) versus number of taps, received signal power, state of polarization (SOP), reach, and bit rate. The modulator consists of two TWMZMs with average $V_\pi L$ and 3-dB bandwidth at 1.5 V DC bias voltage of 2.88 V.cm and 24.5 GHz, respectively. The DP-PAM2 results are one to two order of magnitude better compared to the obtained results in [17]. In addition, results reveal that only 5 taps are required for a 168 Gb/s DP-PAM4 signal using the 6×2 multiple-input multiple-output (MIMO) equalization at the receiver to achieve a BER below the 7% hard-decision forward error correction (HD-FEC) threshold (i.e., 3.8×10^{-3}). Also, we can achieve 112 Gb/s DP-PAM2 over 10 km of SMF at a BER of 1.17×10^{-6} at the worst case state of polarization (SOP). In addition, 168 Gb/s (42

Optics EXPRESS

Gbaud DP-PAM4) is successfully transmitted over 10 km of SMF at a BER below the HD-FEC threshold at 2 dBm received signal power. Finally, we compare the performance of the 6×2 MIMO to a simpler 4×2 MIMO, and discuss the superior performance of the 6×2 MIMO in the presence of SVR imperfections.

The rest of this paper is organized as follows. In section 2, the device details are explained. DC and small-signal characterization are presented in section 3. In section 4, the experimental setup is introduced, and the system-level experimental results for PAM2 and PAM4 modulation formats are presented in section 5. Finally, the paper is concluded in section 6.

2. Device fabrication

The transmitter was fabricated in a multi-project wafer (MPW) run at IME A*STAR on a silicon-on-insulator (SOI) wafer with a 220-nm-thick top silicon layer, a 2-μm-thick buried oxide (BOX) layer, and a high-resistivity 750 Ω-cm silicon substrate using 248 μm lithography. In this transmitter, we leverage our previous series push-pull (SPP) TWMZM designs, where almost all the design parameters of both modulators, such as the p-n junction geometry, doping densities, and the electrode geometry are the same as in [12, 18]. To enable O-band single mode operation, the rib waveguide width was reduced to 400 nm. The modulator length is 4.2 mm with an active length of 3.6 mm. The SPP configuration of the TWMZM lowers the microwave losses and improves modulation bandwidth compared to the conventional dual differential drive scheme. Moreover, one driving RF signal is required per TWMZM which simplifies the operation of the device.

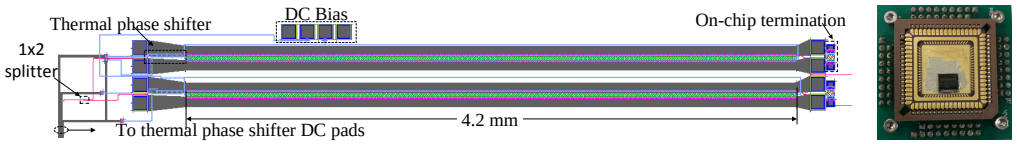

Fig. 1. (a) Layout schematic for the SiP transmitter, and (b) micrograph of the die wirebonded to a chip carrier mounted on a PCB board.

Figure 1(a) shows the layout of the SiP transmitter. The continuous wave (CW) light is coupled to the SiP chip using a focusing grating coupler, where it is then split by a low loss Y-branch [19]. Each branch is connected to one of the TWMZMs. An intentional path imbalance between the modulator arms is added to allow for phase shift measurements [11]. Due to expected fabrication errors, the modulators' transmission spectra are shifted from each other, and a thermal phase shifter is added to one of the arms of each modulator to match the operating bias point of both modulators. The outputs of both modulators were not combined on chip due to the use of booster optical amplifiers (BOAs) which amplify only one state of polarization and hence, polarization combining had to be performed off-chip after optical amplification of each polarization separately. The die was wirebonded to a chip carrier and mounted on a printed circuit board (PCB) for the DC connections (i.e., control signals of thermal phase shifters and bias of the pn junctions) as shown in Fig. 1(b).

3. DC characterization, and small-signal characterization

3.1. DC characterization

The measured transmission spectra for both arms of each modulator at different reverse bias voltages and the extracted phase shift are shown in Fig. 2. At maximum transmission, the fiber-to-fiber insertion loss (IL) is measured to be ~24.5 dB from the input to the output of one of

Optics EXPRESS

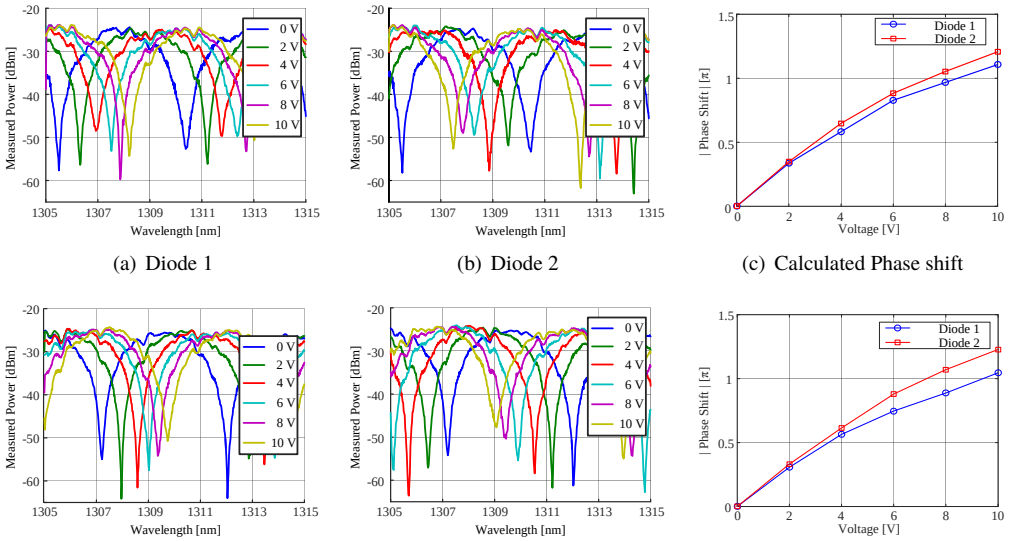

(a) Diode 1 (b) Diode 2 (c) Calculated Phase shift

(d) Diode 1 (e) Diode 2 (f) Calculated Phase shift

Fig. 2. (a) and (b) Transmission spectra for upper modulator diodes, (c) phase shift versus bias voltage for upper modulator diodes, (d) and (e) transmission spectra for lower modulator diodes, and (f) phase shift versus bias voltage for lower modulator diodes

the two modulators. The IL breakdown is as follows: ~10 dB from grating couplers, 3.3 dB from Y-branch (splitting and excess losses), ~7 dB routing losses, and 4.2 dB from the modulator. The high coupling losses can be significantly reduced to be less than 2 dB using low loss edge couplers instead of vertical grating couplers [20–22]. Also, the routing losses can be reduced to less than 0.5 dB using multi-mode rib waveguides for routing instead of 7 dB using single mode strip waveguides [23, 24]. Since the transmission spectra of both modulators are not identical after fabrication as shown in Fig.2, a thermal phase shifter is needed for each modulator to be able to adjust the bias point to quadrature at the operating wavelength.

The phase shift versus voltage is extracted from the transmission spectrum for each arm (diode) of both modulators and shown in Figs. 2(c) and 2(f). A different phase shift is obtained from the two diodes of each modulator under the same applied voltage. This can be attributed to dopant masks misalignment during fabrication [11]. The V_π is approximately 8.25 V and 7.5 V for diodes 1 and 2 for the upper modulator, respectively. Also, the V_π is approximately 9.25 V and 7.1 V for diodes 1 and 2 for the lower modulator, respectively. This indicates an average $V_\pi L$ value of 2.83 V.cm and 2.94 V.cm for the upper and lower modulator, respectively.

3.2. Small-signal characterization

A 50 GHz Keysight lightwave component analyzer and 50 GHz GSSG probes were used to perform the small-signal characterization for both modulators. Figures 3(a) and 3(b) show the electro-optic (EO) S_{21} magnitude response normalized to the response at 1.5 GHz reference frequency for bias voltages of 0 V and 1.5 V. We choose only a 1.5 V bias voltage beside 0 V to do the small-signal characterization as it is the DC bias used in the system experiment as shown in the next section. The 3-dB bandwidth is approximately 17 GHz at 0 V and increases to 25.5 GHz at 1.5 V reverse bias voltage for the upper modulator. Also, the 3-dB bandwidth is approximately 17.5 GHz at 0 V and increases to 23.5 GHz at 1.5 V reverse bias voltage for the lower modulator. The measured electrical-electrical (EE) S_{11} responses for both modulators are

Optics EXPRESS

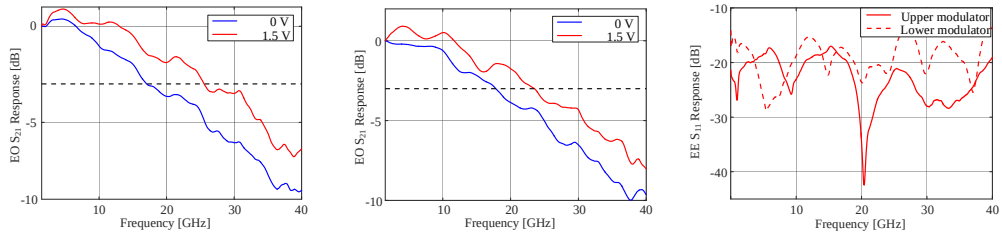

(a) (b) (c)

Fig. 3. (a) EO S_{21} for the upper modulator, (b) EO S_{21} for the lower modulator, and (c) EE S_{11} for both modulators at 1.5 V.

shown in Fig. 3(c). The S_{11} magnitude is well below −10 dB over 40 GHz for both modulators.

4. Experimental setup

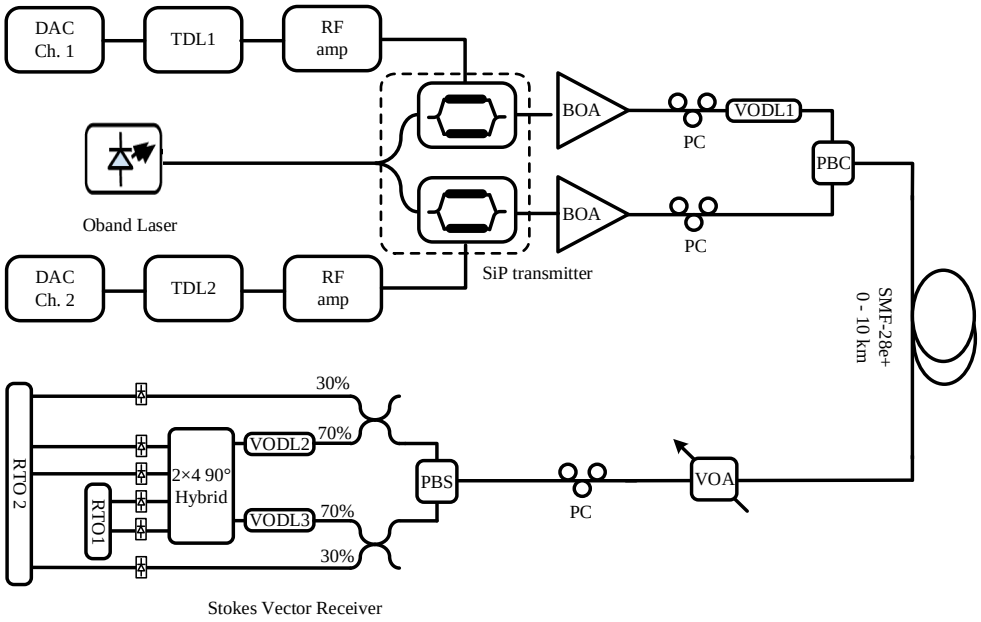

Fig. 4. Experimental setup used to test the SiP modulator. DAC: digital to analog converter, TDL: tunable delay line, BOA: booster optical amplifier, VODL: variable optical delay line, PBC: polarization beam combiner, PC: polarization controller, VOA: variable optical attenuator, PBS: polarization beam splitter, RTO: real time oscilloscope.

Figure 4 introduces the experimental setup. First, transmitter DSP is applied where it includes symbol generation, raised cosine (RC) pulse shaping, a pre-emphasis filter, clipping, and quantization [25]. The pre-emphasis filter is a finite impulse response (FIR) filter found adaptively using the least mean squares (LMS) algorithm after the RF amplifier, and applied at 1 samples per symbol (SPS) on the generated symbols. The number of taps for the pre-emphasis filter is fixed at 75, however 99% of the filter energy is concentrated in only 21 taps. After the transmitter DSP is applied offline, the symbols are loaded into an 8-bit digital-to-analog converter (DAC) running at

Optics EXPRESS

84 GSa/s. Two matched RF tunable delay lines (TDLs) are used before the amplifiers to eliminate the RF skew between both channels including the modulators' skew. Then, the output RF signals are amplified using two 50 GHz RF amplifiers before being applied to the SiP transmitter using a 50 GHz GSSG probe. The driving voltage swing out of the amplifier is dependent on the baud rate, and the roll-off factor used. For example, the peak-to-peak amplitudes of the 28, 42, and 56 Gbaud PAM-4 signals with roll-off factors of 1, 0.55, and 0.3 are 5.6 V, 4.7 V, and 3.1 V, respectively. An O-band laser operating at 1310 nm launches a 13.7 dBm optical carrier into the chip via the input grating coupler. The quadrature point is set using the thermal phase shifter of each modulator. A 1.5 V DC reverse bias voltage is applied to both modulators. This bias voltage was experimentally optimized to get minimum BER where an optimum trade off between the EO bandwidth and V_π is achieved. We reiterate here that the outputs of both modulators are not combined on chip due to the use of single polarization BOAs to compensate for the chip loss. A variable optical delay line (VODL) is added on one of the branches to be able to time align the signals on the two polarizations prior to combining by a polarization beam combiner (PBC). Then, the polarization multiplexed signal is launched into various lengths of SMF (Corning SMF-28e+). A variable optical attenuator (VOA) is added to sweep the received signal power. The optical signal is then received by the SVR shown in Fig. 4, where the coupler splitting ratios have been chosen to be 70/30, close to the optimum ratio of 67/33 required for SOP independent operation [26]. A polarization controller (PC) is added before entering the receiver to vary the SOP and verify the performance dependence on received SOP. Since balanced photodetectors (PDs) were not available in the O-band, single ended PDs are used in the experiment. The PDs have a bandwidth of 35 GHz and are followed by a trans-impedance amplifier stage. The six signals out of the PDs are sampled at 80 GSa/s by two 33 GHz real time oscilloscopes (RTOs) and stored for offline processing to be applied on the received electrical signals. The receiver DSP consists of resampling to 2 SPS, 6×2 real-valued multiple-input multiple-output (MIMO) equalization, symbol decision, and bit error counting. After resampling at 2 SPS, we feed the six output waveforms from the PDs to the MIMO DSP. The desired estimated outputs are the two intensities on both polarization, i.e., $|E_x^2|$ and $|E_y^2|$, and the taps are updated adaptively using the LMS algorithm. The MIMO DSP task is for polarization demultiplexing and residual inter-symbol interference (ISI) mitigation.

5. Experimental results

In this section, we present the experimental results for the LMS convergence, PAM2 and PAM4 modulation formats. We consider the 7% overhead HD-FEC threshold with uncorrected input BER of 3.8×10^{-3}.

5.1. LMS convergence

In Fig. 5, we study the LMS convergence for a 42 Gbaud DP-PAM4 signal in the B2B case. In Fig. 5(a), we calculate the transient BER to assess the convergence speed of the LMS algorithm used to adapt the taps of the 6×2 MIMO that operates on the SVR outputs for different values of LMS step size. For this study, the number of taps is kept constant at 55 and the transient BER is evaluated by counting errors in a smaller window of 200000 symbols that we slide by steps of 2500 symbols. As expected, using a large step size will cause the LMS to converge faster however it may converge to a higher steady state BER due to the excess mean squared error at steady state; a characteristic of the LMS algorithm when choosing an excessively large step size [27]. For example, using a step size of 0.01 causes the LMS to converge on a steady state BER of 2.7×10^{-3}. Also, the LMS with a step size of 0.001 converges after 5000 symbols with a steady state BER of $\sim 3 \times 10^{-4}$, which gives the best trade-off between the convergence speed and the steady state BER. Decreasing the step size further decreases significantly the convergence speed without improving the steady state BER, where the LMS didn't converge using a step size of

Optics EXPRESS

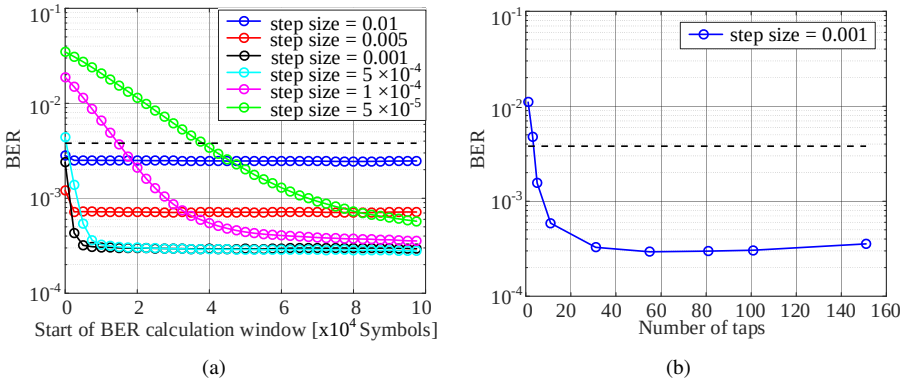

Fig. 5. LMS convergence for the 168 Gb/s DP-PAM4 signal in the B2B case for (a) different LMS step size values and (b) different number of taps.

5×10^{-5} even after 100000 symbols.

Next, the steady state BER versus the number of LMS taps is shown in Fig. 5(b) for a fixed step size of 0.001. The number of taps is varied from a single tap to 151 taps, where a single tap means the MIMO is a 6×2 matrix with no temporal length. Hence, the MIMO can de-rotate the polarization and correct any imbalance between the outputs but will not equalize for any ISI. It can be observed that only 5 taps are required to have a BER below the HD-FEC threshold. Increasing the number of taps improves the BER where it reaches $\sim 3 \times 10^{-4}$ at 55 taps. Moreover, the BER slightly degrades when increasing the number of taps to 101 and 155 due to the additional adaptation noise from the unwanted extra taps. For the rest of the results, we fixed the step size and number of taps to 5×10^{-4} and 55 taps, respectively.

5.2. PAM2 performance

Figures 6(a) and 6(b) show the BER and SNR performance versus received signal power of the 112 Gb/s DP-PAM2 signal at different SOPs in the B2B case. It can be observed that changing the SOP from completely aligned (0^o SOP) to completely misaligned (45^o SOP) has a negligible effect on the performance. This indicates the successful restoration of the transmitted dual-polarization signal using the 6×2 MIMO DSP block and proves the receiver is SOP independent as mentioned in the experimental setup. Approximately -5.5 dBm is needed to achieve a BER below the HD-FEC for a 112 Gb/s DP-PAM2 signal at any SOP in the B2B case. Increasing the received power further enhances the BER performance until reaching a BER of 1.17×10^{-6}, where the length of the captured frames is not enough to accurately measure the BER below 1×10^{-6}. Hence, we show the SNR versus received signal power in Fig. 6(b), where the BER is estimated to be lower than 1×10^{-6} at 0 dBm received signal power [28]. The SNR increases to 17 dB at 3 dBm received signal power, and then saturates with increased received power. In this regime, the SNR is no longer limited by the received signal power and is completely governed by the transmitter signal integrity. In Fig. 6(c), we present the BER performance versus received power over various reaches at random SOP. It can be observed that the degradation of the BER due to fiber transmission is minimal at equal received power for the 2 km case compared to the B2B case. However, the BER performance degrades when the reach is increased to 10 km. A BER below the HD-FEC threshold is achieved at less than -5.5 dBm received signal power for the B2B and 2 km cases, and increases to -4.5 dBm for the 10 km case. Although this behavior is not expected in the O-band where chromatic dispersion is less significant, we observe approximately 1.5 dB SNR reduction in the 10 km case. Our explanation of this SNR reduction is based on the

Optics EXPRESS

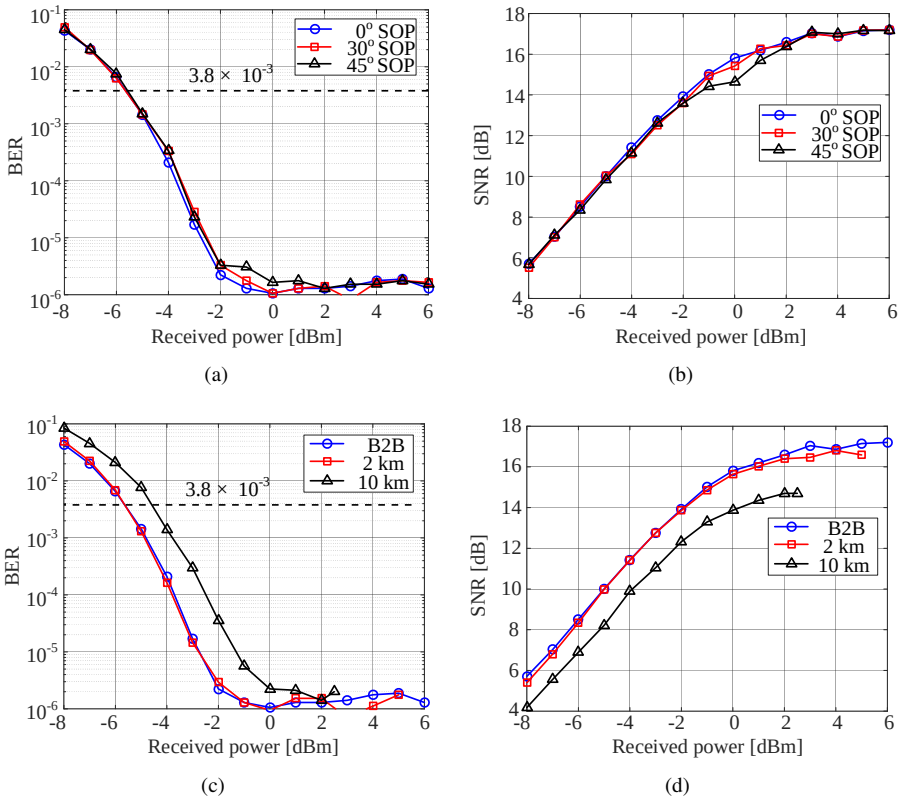

Fig. 6. BER and SNR performance for the 112 Gb/s DP-PAM2 signal versus received power for the B2B case at different SOPs (a-b) and over different reaches at random SOP (c-d).

performance of the BOA which receives an input optical signal power exiting the SiP chip of ~ -14.5 dBm. At low input signal powers, we observed a significant amount of intensity noise in the received signal after fiber propagation over 10 km which was not significant in the B2B and 2 km cases. In contrast, the intensity noise almost vanishes when the input signal power to the BOA is above -5 dBm. Moreover, we find a dependency of this noise on the BOA current and temperature, where the noise increases with the BOA current, and decreases with increases in temperature. Hence, for the 2 km and 10 km curves, we optimized the temperature and BOA current to decrease the noise originating from the BOA after fiber propagation while having sufficient gain to amplify the input signal. We conclude that parasitic tone leakage and chirp from the BOAs is the reason for the additional intensity noise observed at the receiver, where it is pronounced after fiber propagation due to the interaction between tone leakage, chirp, and fiber dispersion. The effect is more significant on the performance of the PAM4 results as shown in the next section. Using a polarization insensitive amplifier as a pre-amplifier at the receiver side, e.g., a single praseodymium-doped fiber amplifier (PDFA) should resolve this problem which was not available at the time of the experiment. Furthermore, an optical amplifier would not be used in deployed systems because packaged transceivers, including lasers, will have lower insertion losses.

Optics EXPRESS

5.3. PAM4 performance

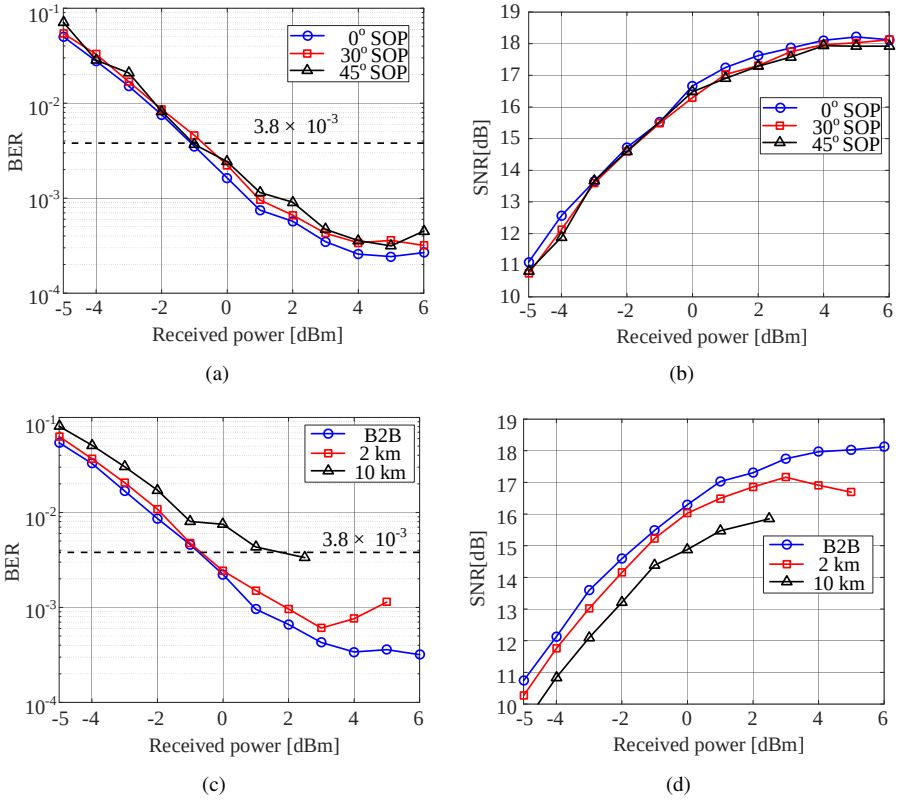

Fig. 7. BER and SNR performance for the 168 Gb/s DP-PAM4 signal versus received power for the B2B case at different SOPs (a-b) and random SOP over different reaches (c-d).

We report the BER and SNR performance of 168 Gb/s (42 Gbaud) DP-PAM4 signal versus received power in Fig. 7. Similar to the DP-PAM2 results, we show that changing the SOP has a negligible effect on the performance as shown in Figs. 7(a) and 7(b). It can be observed in Fig. 7(a) that approximately −1 dBm received signal power is needed to achieve a BER below the HD-FEC at any received SOP. In Figs. 7(c) and 7(d), we present the performance at random SOP for different reach values. At 2 km reach, we notice a slight degradation in the BER and SNR performance compared to the B2B case. This is attributed to the BOA behavior as explained in the previous section. Furthermore, a higher driving BOA current is used for the 4 and 5 dBm received signal power points in Figs. 7(c) and 7(d). This results in the reduction of the SNR and consequently the BER increases due to the increased noise. For the 10 km reach, the SNR decreases by approximately 1.5 dB compared to the B2B case as shown in Fig. 7(d). Hence, the BER increases and approximately 2 dBm received signal power is required to achieve a BER below the HD-FEC threshold. In the 10 km reach cases shown in Figs. 7(c) and 7(d) the maximum received signal power achievable was approximately 2.5 dBm based on maximum output power limitations of the BOA.

Optics EXPRESS

5.4. BER performance versus bit rate

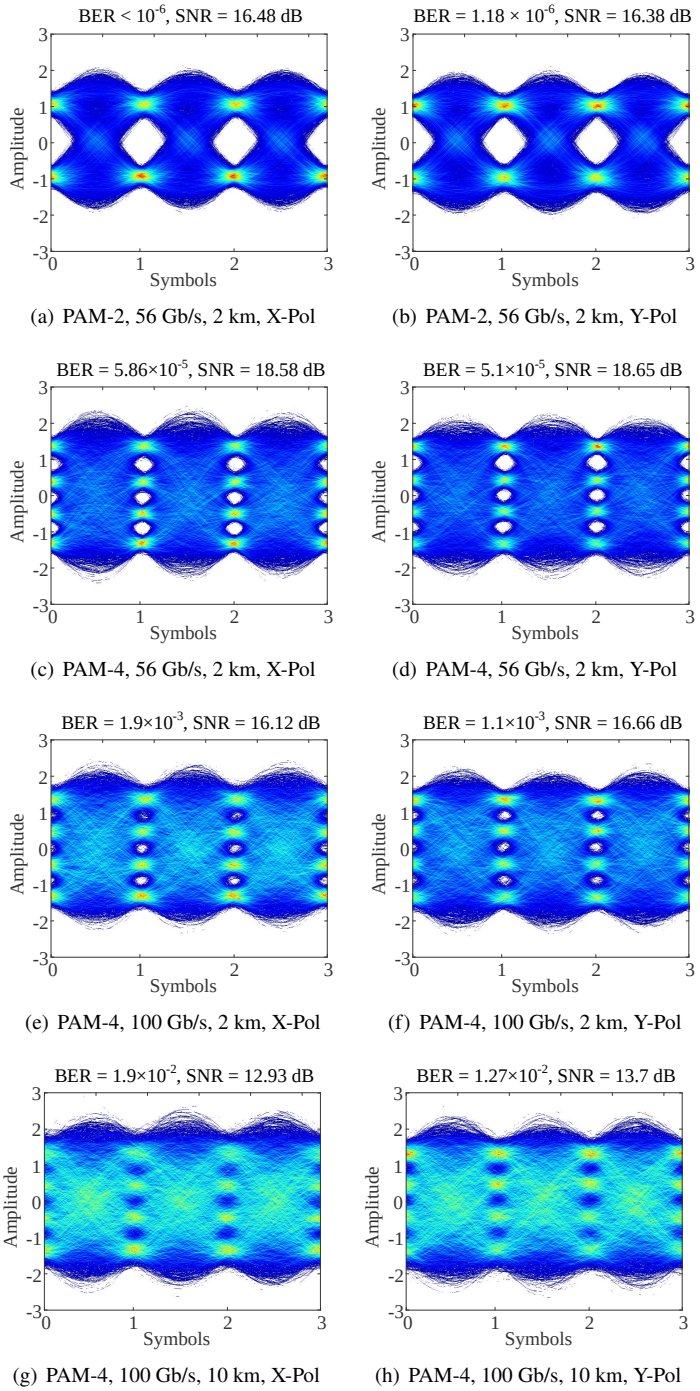

(a) PAM-2, 56 Gb/s, 2 km, X-Pol (b) PAM-2, 56 Gb/s, 2 km, Y-Pol

(c) PAM-4, 56 Gb/s, 2 km, X-Pol (d) PAM-4, 56 Gb/s, 2 km, Y-Pol

(e) PAM-4, 100 Gb/s, 2 km, X-Pol (f) PAM-4, 100 Gb/s, 2 km, Y-Pol

(g) PAM-4, 100 Gb/s, 10 km, X-Pol (h) PAM-4, 100 Gb/s, 10 km, Y-Pol

Fig. 8. Eye diagrams for PAM2 and PAM4 modulation formats obtained after receiver DSP at different bit rates and reaches.

Optics EXPRESS

Figure 8 presents eye diagrams for the DP-PAM2 and DP-PAM4 signals at different bit rates after receiver DSP. In Figs. 8(a) and 8(b), a 112 Gb/s (56 Gb/s per polarization) DP-PAM2 is shown after 2 km of SMF, where a clear open eye diagram is observed. Moreover, it is interesting to show the performance of the same signal bit rate (112 Gb/s) using the PAM4 modulation format which operates at half the symbol rate of the DP-PAM2 signal as shown in Fig. 8(c) and 8(d). The eye diagram of the 28 Gbaud signal shows a good eye opening, with a BER of 5.86×10^{-5} and 5.1×10^{-5} for the X-pol and Y-pol, respectively. As expected, increasing the symbol rate further degrades the received signal quality, however 200 Gb/s is still achievable below the HD-FEC after 2 km of SMF with a relatively open eye diagram. Increasing the transmission to 10 km significantly degrades the performance for the 200 Gb/s compared to the 2 km reach due to the BOA behavior as discussed in the previous section. To re-iterate here, this problem is not related to the SiP transmitter but related to the BOA followed by SMF. This problem will be removed if the BOAs are used as pre-amplifiers after the polarization beam splitter or replaced by a polarization insensitive PDFA.

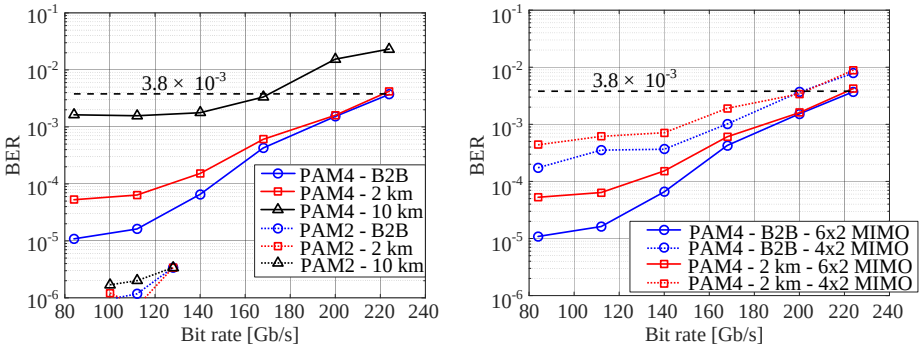

Fig. 9. (a) BER versus bit rate for PAM2 and PAM4 modulation formats for B2B, 2 km, and 10 km reaches, and (b) BER versus bit rate for PAM4 modulation format using 6×2 and 4×2 MIMO.

Figure 9(a) presents the BER versus the bit rate at different reaches for PAM2 and PAM4 modulation formats. The received signal power was kept at 3 dBm for the B2B and the 2 km curves, and at 2.5 dBm (the maximum available power based on BOA performance) for the 10 km curves. For the PAM2 signal, a bit rate up to 128 Gb/s over as much as 10 km can be transmitted at a BER below 4×10^{-6}. For the PAM4 signal, 224 Gb/s can be achieved in the B2B configuration below the HD-FEC threshold, where the BER increases to 4×10^{-3} after 2 km reach. Also, 200 Gb/s transmission over 2 km can be achieved at a BER of 1.6×10^{-3}. Finally, only 168 Gb/s can be transmitted over 10 km with BER below the HD-FEC threshold.

As discussed in Section 4, we used 6×2 MIMO equalization for the polarization demultiplexing and residual ISI mitigation in all the previous results, where we feed the 6 electrical outputs from the real-time scopes directly to the MIMO. A simpler 4×2 MIMO can be used instead, where the differential pair outputs are first subtracted before the MIMO equalization. In Fig. 9(b), we compare the 6×2 and 4×2 MIMO equalization schemes for the DP-PAM4 modulation format in the B2B and 2 km cases. In our experiment, we used a custom-built O-band hybrid which had insertion losses of 6.5 dB, 7.2 dB, 6.38 dB, and 6.42 dB from input port 1 to the output ports, and 6.38 dB, 6.51 dB, 6.63 dB, and 6.87 dB from input port 2 to the output ports. Also, we used six single ended PDs since no balanced PDs were available in the O-band which have unequal conversion factors (V/W). The 6×2 MIMO is given by the following equation if we ignore the

Optics EXPRESS

temporal length of the filters:

$$\begin{bmatrix} |E_{\hat{x}}|^2 \\ |E_{\hat{y}}|^2 \end{bmatrix} = \begin{bmatrix} h_{11} & h_{21} & h_{31} & h_{41} & h_{51} & h_{61} \\ h_{12} & h_{22} & h_{32} & h_{42} & h_{52} & h_{62} \end{bmatrix} \begin{bmatrix} |E_x^r|^2 \\ |E_y^r|^2 \\ S_{2p}^r \\ S_{2n}^r \\ S_{3p}^r \\ S_{3n}^r \end{bmatrix}$$

where $|E_{\hat{x}}|^2$ and $|E_{\hat{y}}|^2$ are the desired outputs, h_{ij} is the tap coefficient between input i and output j to the MIMO, $|E_x^r|^2$ and $|E_y^r|^2$ are the received direct detection outputs, S_{2p}^r and S_{2n}^r are the differential pairs for the S_2 parameter, and $S_{3p}^r$and S_{3n}^r are the differential pairs for the S_3 parameter. For the 4×2 MIMO, we subtract the two differential pair electrical outputs first and then feed them to the MIMO given by:

$$\begin{bmatrix} |E_{\hat{x}}|^2 \\ |E_{\hat{y}}|^2 \end{bmatrix} = \begin{bmatrix} h_{11} & h_{21} & h_{31} & h_{41} \\ h_{12} & h_{22} & h_{32} & h_{42} \end{bmatrix} \begin{bmatrix} |E_x^r|^2 \\ |E_y^r|^2 \\ S_2^r \\ S_3^r \end{bmatrix}$$

where S_2^r and S_3^r are the reconstructed stokes parameters from the differential waveforms after the direct detection terms are canceled.

Hence, the 6×2 MIMO will be capable of compensating the SVR imperfections e.g., power imbalance and the skew between the SVR outputs, and unequal PD responsivity. However, the simpler 4×2 MIMO will not be able to correct them since the differential pairs are subtracted before the MIMO and any residual common mode terms will degrade the performance. As a result, we can observe a degradation in the BER when the 4×2 MIMO is used as shown in Fig. 9(b). For example, the BER is $\sim 6 \times 10^{-5}$ using the 6×2 MIMO and increases to $\sim 6 \times 10^{-4}$ when using the 4×2 MIMO for 112 Gb/s DP-PAM4 in the 2 km case.

6. Conclusion

A dual-polarization O-band SiP transmitter for intra-datacenter optical interconnects is experimentally demonstrated. The transmitter has an average $V_\pi L$ and a bandwidth at 1.5 V reverse bias voltage of 2.88 V.cm and 24.5 GHz, respectively. We test the transmitter for DP-PAM2 and DP-PAM4 formats using a DD-SVR versus various parameters. Results reveal that 112 Gb/s DP-PAM2 can be transmitted over as much as 10 km of SMF at a BER below 10^{-5} at −1 dBm received signal power and random SOP. Also, 168 Gb/s (42 Gbaud) DP-PAM4 signal can be transmitted over 2 km and 10 km at a BER below the HD-FEC at 0 dBm and 2 dBm, respectively. In addition, 224 Gb/s and 200 Gb/s DP-PAM4 is successfully received at a BER below the 7% HD-FEC in the B2B and 2 km cases, respectively. Finally, we explain the superior performance of the 6×2 MIMO compared to the 4×2 in the presence of SVR imperfections.

Acknowledgments

We gratefully acknowledge CMC Microsystems for enabling fabrication, and providing access to simulation and CAD tools. We also thank Prof. Chen in McGill University for his helpful discussion.